CHIN. PHYS. LETT. Vol. 38, No. 3 (2021) 030301

Two-Dimensional Quantum Walk with Non-Hermitian Skin Effects

Tianyu Li(李天宇)[1], Yong-Sheng Zhang(张永生)[1,2*], and Wei Yi(易为)[1,2*]

[1]*CAS Key Laboratory of Quantum Information, University of Science and Technology of China, Hefei 230026, China*
[2]*CAS Center For Excellence in Quantum Information and Quantum Physics, Hefei 230026, China*

(Received 3 October 2020; accepted 8 December 2020; published online 2 March 2021)

We construct a two-dimensional, discrete-time quantum walk, exhibiting non-Hermitian skin effects under open-boundary conditions. As a confirmation of the non-Hermitian bulk-boundary correspondence, we show that the emergence of topological edge states is consistent with the Floquet winding number, calculated using a non-Bloch band theory, invoking time-dependent generalized Brillouin zones. Further, the non-Bloch topological invariants associated with quasienergy bands are captured by a non-Hermitian local Chern marker in real space, defined via the local biorthogonal eigenwave functions of a non-unitary Floquet operator. Our work aims to stimulate further studies of non-Hermitian Floquet topological phases where skin effects play a key role.

DOI: 10.1088/0256-307X/38/3/030301

Non-Hermitian topological phases arise in open systems with non-Hermitian effective Hamiltonians,[1] and can exhibit remarkable properties with no counterparts in Hermitian settings. In this context, one of the most intensively discussed phenomena is the breakdown of conventional bulk-boundary correspondence,[2–11] which can be restored by means of a non-Bloch band theory to account for the localization of nominal bulk eigenstates near boundaries,[6–17] known as non-Hermitian skin effects. So far, non-Hermitian skin effects and the commensurate non-Hermitian bulk-boundary correspondence have been experimentally observed in topoelectric circuits[18,19] and metamaterials,[20] as well as using photons.[21,22] These experiments have explored the sensitivity of eigenenergy spectra to boundary conditions, the localization of bulk wave functions near boundaries, and the correspondence between topological edge states with non-Bloch topological invariants. However, an experimental demonstration of non-Hermitian skin effects in higher-dimensional quantum mechanical systems is still lacking, for want of a readily accessible methodology.

In this work, we propose a two-dimensional, discrete-time quantum walk, which features non-Hermitian skin effects, and is amenable to existing control protocols on quantum simulation platforms such as photons and cold atoms. An exemplary Floquet system, discrete-time quantum walks, subject to appropriate design, acquire topological properties,[23–35] characterized by a pair of Floquet winding numbers, which, in two dimensions, are intimately connected to the Chern numbers of the corresponding quasienergy bands.[36] For our proposed quantum walk, we find that the topological invariants capable of characterizing topological edge states should be calculated via a non-Bloch extension of the Floquet winding numbers, defined on a generalized Brillouin zone which is time-dependent within one driving period. Furthermore, we show that non-Bloch topological invariants of the system can be revealed via a non-Hermitian local Chern marker in real space, which suggests the possibility of probing non-Bloch topological invariants in the bulk of the system using quasi-local measurements. Our study offers the interesting prospect of probing non-Hermitian skin effects and non-Bloch topological invariants in higher-dimensional non-Hermitian topological systems, and enriches the understanding of non-Hermitian Floquet topological phases.[12,37,38]

Model and Quasi-Energy Spectrum. We consider a discrete-time, non-unitary quantum walk on a bipartite square lattice, with the Floquet operator reading

$$U = T_4(\theta_1)T_3(-\theta_2)M(\gamma)T_2(-\theta_2)T_1\left(\theta_1 - \frac{\pi}{2}\right), \quad (1)$$

where $T_j(\theta) = e^{i\theta\sigma_y}$ $(j = 1, 2, 3, 4)$, imposing rotations in the basis of adjacent sublattice sites $\{|A\rangle, |B\rangle\}$ according to the bonds and sequence illustrated in Fig. 1. Here σ_i $(i = x, y, z)$ are the Pauli matrices in the basis of sublattice sites $\{|A\rangle, |B\rangle\}$, with $\sigma_y = -i|A\rangle\langle B| + i|B\rangle\langle A|$. Non-unitarity is introduced through the gain-loss operator $M = e^{\gamma\sigma_z}$,[21,31,32] such that wave functions on sublattice sites A (B) are subject to gain (loss) in each time step. Here γ is the gain-loss parameter.

Based on recent experimental progress with respect to topological quantum walks with

Supported by the National Natural Science Foundation of China (Grant Nos. 11974331, 11674306, and 61590932), and the National Key R&D Program (Grant Nos. 2016YFA0301700 and 2017YFA0304100).
*Corresponding authors. Email: yshzhang@ustc.edu.cn; wyiz@ustc.edu.cn
© 2021 Chinese Physical Society and IOP Publishing Ltd

photons[29–35] or cold atoms,[39] such a design is accessible under the flexible control of these systems. This is particularly the case with single photons, where one-dimensional topological quantum walks with non-Hermitian skin effects have recently been implemented.[21] Specifically, the operators T_i can be directly translated to a combination of coin and shift operators used for photonic quantum walks.[21] As a concrete example, we have $T_2(-\theta_2) = SR(\theta_2)S^\dagger$, where the shift ($S$) and coin ($R$) operators are respectively defined as $S = \sum_m |m+1\rangle\langle m| \otimes |A\rangle\langle B| + |m\rangle\langle m| \otimes |B\rangle\langle A|$ and $R(\theta) = \mathbf{1}_m \otimes e^{i\theta\sigma_y}$, with $\mathbf{1}_m$ the identity operator in the unit-cell space. Here, the unit cells are identified as adjacent sublattice sites bonded by T_2, as shown in Fig. 1. Compared to Ref. [21], it is apparent that our protocol for a two-dimensional quantum walk requires more operations per time step. This represents a major difficulty for its implementation; however, this could be overcome, for instance, by employing a time-multiplexing construction.[40]

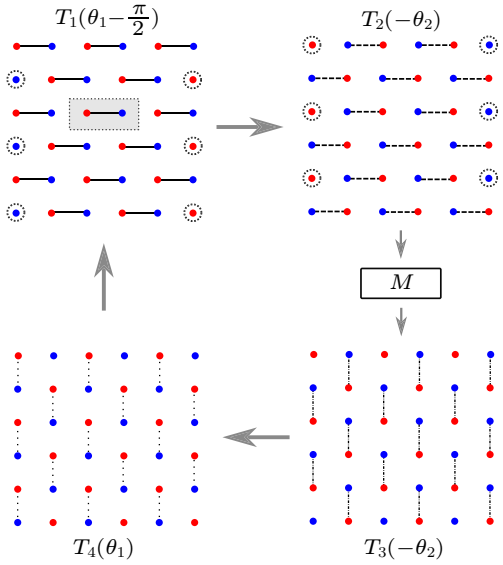

Fig. 1. Discrete-time quantum walk on a bipartite two-dimensional lattice. For each driving period, rotations T_j (see the text for definition), are applied sequentially on neighboring sublattice sites A (red) and B (blue) in a spatially homogeneous fashion. The non-unitary gain-loss operator M is inserted between T_2 and T_3 in each period. The quantum walk is characterized by the angle parameters (θ_1, θ_2) in accordance with Eq. (1). The shaded area indicates a unit cell for relevant calculations throughout this work. Under the open-boundary condition, uncoupled sublattice sites at the boundaries (circled) at a given sub-step T_j are left unchanged.

As we demonstrate below, the Floquet operator in Eq. (1) drives a non-unitary quantum walk with non-Hermitian skin effects. However, to characterize Floquet winding numbers that account for topological edge states, a generalized *time-dependent* Brillouin zone would be needed, in sharp contrast to previous studies.

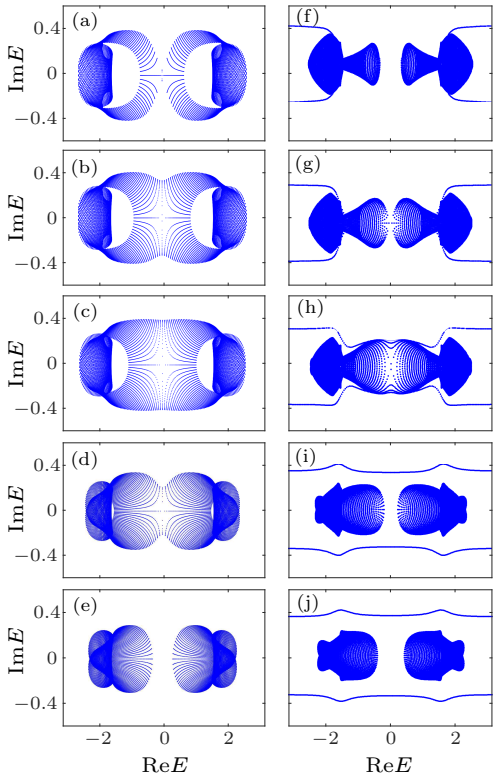

Fig. 2. Typical energy spectra of the system under PBC [(a)–(e)] and OBC [(f)–(j)], respectively, with the parameters: [(a),(f)] $\theta_1 = 0.78\pi$, [(b),(g)] $\theta_1 = 0.806\pi$, [(c),(h)] $\theta_1 = 0.83\pi$, [(d),(i)] $\theta_1 = 0.895\pi$, [(e),(j)] $\theta_1 = 0.92\pi$. For all subplots, we take $\theta_2 = 1.59\pi$ and $\gamma = 0.4$, with the lattice size given by $L_x \times L_y = 160 \times 160$. Here, L_x (L_y) is the number of lattice sites (including all sublattice sites) along the x (y) direction.

A prominent feature of non-Hermitian systems with skin effects is the sensitive dependence of the energy spectrum on boundary conditions. In Fig. 2 we show the quasienergy spectra E, associated with the Floquet Hamiltonian $H_{\rm F}$, as defined via $U = e^{-iH_{\rm F}}$ (with a branch cut at $E = \pi$), where two distinct boundary conditions are considered: a periodic boundary condition along both x and y directions [Figs. 2(a)–2(e), labeled as PBC]; an open boundary condition in the x direction but which is periodic along y [Figs. 2(f)–2(j), labeled as OBC]. Under the OBC, uncoupled sublattice sites at the boundaries during a given sub-step are left unchanged (see Fig. 1). As typical ones of non-Hermitian Floquet topological phases, two quasienergy bandgaps near $\mathrm{Re}E = 0$ and $\mathrm{Re}E = \pi$ are identified on the complex plane, where edge states can appear under OBC. With changing parameters, these bandgaps can close [Figs. 2(a) and 2(g) at $\mathrm{Re}E = 0$] and open up again [Figs. 2(e), 2(i) and 2(j)], but gapless regimes generally exist [Figs. 2(b), 2(c), 2(d) and 2(h)], which is a common feature for many two-dimensional non-Hermitian topological systems.[7] On the basis of the

way the band gaps close and open, we identify these as line gaps, according to the definition in Ref. [41]. A particularly important point to note is that the gap closing point occurs at distinct parameters under different boundary conditions [Figs. 2(a) and 2(g)], suggesting the breakdown of conventional bulk-boundary correspondence. This is more explicitly illustrated in Figs. 2(d) and 2(i), where the system under PBC is gapless near Re$E = 0$, prohibiting the definition of topological invariants, whereas the same gap is open, and a pair of in-gap edge states appear, under OBC.

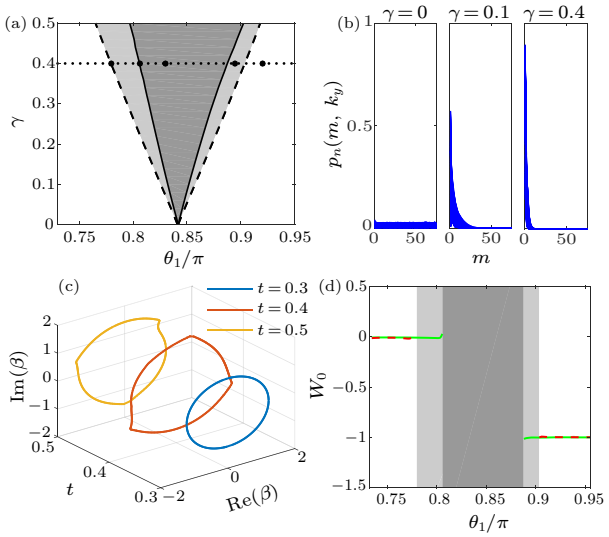

Fig. 3. (a) Gapless regions (for the gap near Re$E = 0$) in a parameter space spanned by γ and θ_1. The light (dark) shaded region denotes gapless regions under PBC (both PBC and OBC). The five black dots indicate the parameters used for different rows in Fig. 2, from top to bottom in the same sequential order. (b) Normalized spatial probability distributions, $p_n(m,k_y) = \sum_{s=A,B} |\langle m,s|\psi_{n,R}\rangle_{k_y}|^2$, for all the eigenstates of U under OBC, superimposed in the plot. Here $|m,s\rangle_{k_y}$ indicates the sublattice state, s, of the mth unit cell along the x direction. $|\psi_{n,R}\rangle_{k_y}$ is the nth right eigenstate of U under OBC for a given k_y. We adopt the parameters $\theta_1 = 0.7\pi$, $k_y = 0.45\pi$ and varying γ, under the normalization condition $\sum_m p_n(m,k_y) = 1$. For our calculation, we take 76 unit cells (labeled as m) along the x direction. Here, all right eigenstates are localized near the left edge, but may localize on the opposite edge, given other parameters. (c) Generalized Brillouin zones, characterized by β on the complex plane, at different times within one driving period, with $\theta_1 = 0.78\pi$, $k_y = 0.45\pi$ and $\gamma = 0.4$. (d) Non-Bloch Floquet winding number $\tilde{W}_0$ and Bloch winding number W_0 for $\gamma = 0.4$. The green solid (red dashed) line shows the calculated non-Bloch (Bloch) winding number $\tilde{W}_0$ (W_0), and the shaded regions denote gapless regions similar to (b). For all cases, we fix $\theta_2 = 1.59\pi$, where the band gap near Re$E = \pi$ remains open with $\tilde{W}_\pi = -1$.

To explore the mismatch in the quasienergy spectrum under different boundary conditions, in Fig. 3(a), we show the gap-closing points and gapless regions under both boundary conditions in the parameter space of γ and θ_1. It appears that the gapless region is larger under the PBC, and the mismatch of gap closing points under different boundary conditions increases with larger non-Hermiticity. This behavior is accompanied by non-Hermitian skin effects [see Fig. 3(b)], with all eigenstates localized at the boundaries, which, according to the non-Bloch band theory, induce the breakdown of Hermitian bulk-boundary correspondence, giving rise to the sensitivity of gap-closing parameters with respect to boundary conditions.[2–6] A natural question then is whether the non-Bloch band theory should restore the bulk-boundary correspondence in our Floquet dynamics?

Non-Bloch Floquet Winding Number. As discussed in Ref. [36], in a two-dimensional Floquet topological system, the bulk-boundary correspondence is governed by the Floquet winding numbers, which are related to Chern numbers of different quasienergy bands in a straightforward manner. Here, we show that a non-Hermitian bulk-boundary correspondence can be established through the introduction of non-Bloch Floquet winding numbers, defined over the generalized Brillouin zone, which is conceptually similar to the static case.

To define the Floquet winding number, we first rewrite the Floquet operator in momentum space, in terms of a time-dependent effective Hamiltonian $H(\boldsymbol{k},t)$,

$$U(\boldsymbol{k}) = \mathcal{T}e^{-i\int_0^1 H(\boldsymbol{k},t')dt'}, \tag{2}$$

where $\mathcal{T}$ is the time-ordering operator. The formally complicated $H(\boldsymbol{k},t)$ can be constructed in a stroboscopic fashion, by dividing each Floquet driving period (taken as unit time) into five steps (see the Supplemental Information). A time-period operator $U_\epsilon(\boldsymbol{k},t)$ ($\epsilon \in \{0,\pi\}$) is then introduced as follows:[36]

$$U_\epsilon(\boldsymbol{k},t) = \begin{cases} \mathcal{T}e^{-2i\int_0^t H(\boldsymbol{k},2t')dt'}, & 0 \le t < \frac{1}{2}, \\ V_\epsilon(\boldsymbol{k},2-2t), & \frac{1}{2} \le t \le 1, \end{cases} \tag{3}$$

where $V_\epsilon(\boldsymbol{k},t) = e^{-iH_\epsilon^{\rm eff}(\boldsymbol{k})t}$, with $H_\epsilon^{\rm eff}(\boldsymbol{k}) = i\ln_\epsilon U(\boldsymbol{k})$. The subscript ϵ indicates that a branch cut at ϵ is taken when evaluating $\ln_\epsilon$. The Floquet winding number is then defined as given in Ref. [36],

$$W_\epsilon = \frac{1}{8\pi^2}\int dtdk_xdk_y \cdot {\rm Tr}(U_\epsilon^{-1}\partial_t U_\epsilon[U_\epsilon^{-1}\partial_{k_x}U_\epsilon, U_\epsilon^{-1}\partial_{k_y}U_\epsilon]). \tag{4}$$

For completeness, we also define the Chern number of a given band

$$C = \frac{1}{2\pi i}\int dk_xdk_y {\rm Tr}(\hat{P}_{\boldsymbol{k}}[\partial_{k_x}\hat{P}_{\boldsymbol{k}}, \partial_{k_y}\hat{P}_{\boldsymbol{k}}]), \tag{5}$$

where the operator $\hat{P}_{\boldsymbol{k}} = |\psi_{\rm R}(\boldsymbol{k})\rangle\langle\psi_{\rm L}(\boldsymbol{k})|$ is the projection onto a given quasienergy band, for instance the band within the range $-\pi <$ Re$E < 0$ or that in the range $0 <$ Re$E < \pi$. Here, $|\psi_{\rm L(R)}(\boldsymbol{k})\rangle$ is the left (right) eigenstate of the relevant band, with $U(\boldsymbol{k})|\psi_{\rm R}(\boldsymbol{k})\rangle =$

$\lambda_{\boldsymbol{k}}|\psi_{\rm R}(\boldsymbol{k})\rangle$ and $U^{\dagger}(\boldsymbol{k})|\psi_{\rm L}(\boldsymbol{k})\rangle = \lambda^{*}_{\boldsymbol{k}}|\psi_{\rm L}(\boldsymbol{k})\rangle$, and $\lambda_{\boldsymbol{k}}$ is the eigenvalue of $U(\boldsymbol{k})$. These eigenstates further satisfy the biorthonormal conditions $\langle\psi_{\rm L}(\boldsymbol{k})|\psi_{\rm R}(\boldsymbol{k'})\rangle = \delta_{\boldsymbol{k},\boldsymbol{k'}}$, where $\delta_{\boldsymbol{k},\boldsymbol{k'}}$ is the Kronecker delta.

For a unitary quantum walk with $\gamma = 0$, the winding number W_0 (W_π) dictates the number of edge states on a given edge and within the gap at ϵ, according to the bulk-boundary correspondence of a two-dimensional Floquet system. The difference between these winding numbers corresponds to the Chern number of the quasienergy band between the relevant gaps.[36] For instance, $W_0 - W_\pi$ ($W_\pi - W_0$) corresponds to the Chern number of the left (right) band with Re$E < 0$ (Re$E > 0$) (see Fig. 2).

In the non-unitary case with finite γ, topological edge states appearing on the boundaries do not always have a correspondence in Floquet winding numbers calculated under the PBC. Specifically, as shown in Figs. 2(d) and 2(i), when the system is gapless near ϵ ($\epsilon = 0, \pi$) under the PBC, imposing an OBC can open up the same gap, within which topological edge states emerge, indicating the breakdown of the conventional bulk-boundary correspondence.

To account for these boundary-dependent topological edge states and restore the bulk-boundary correspondence, we resort to the non-Bloch band theory, where non-Bloch topological invariants are evaluated over a generalized Brillouin zone, based on the non-Bloch nature of the bulk eigenwave functions under the OBC. For the strip-geometry considered here, the Bloch phase factor e^{ik_x} of the bulk eigen wave functions along the x direction is replaced by $\beta(p_x, k_y, t) := |\beta(p_x, k_y, t)|e^{ip_x}$, where p_x is a phase parameter. The time dependence of $\beta(p_x, k_y, t)$ derives from the time-period operator $U_\epsilon(\boldsymbol{k}, t)$, and is directly related to the micromotion of the Floquet dynamics. This is in sharp contrast to the one-dimensional quantum walk in Ref. [21], where the presence of chiral symmetry enables a simplified characterization of the Floquet winding number with time-independent β.[42]

For our case, at any given time t, within one driving period, when the parameters (p_x, k_y) vary, the permitted values of $\beta(p_x, k_y, t)$, dictated by the quasi-energy spectrum through the eigen equations of U_ϵ, form a closed trajectory on the complex plane, representing the generalized Brillouin zone at time t [see Fig. 3(c) and the Supplemental Information]. The non-Bloch Floquet winding numbers, $\tilde{W}_\epsilon$, are then evaluated by making the substitution $(k_x, k_y) \to [p_x - i\ln_\epsilon[|\beta(p_x, k_y, t)|], k_y]$ in Eq. (4), where the time dependence is to be integrated over one period.

We show the calculated non-Bloch Floquet winding numbers in Fig. 3(d), where the light (dark) shaded region indicates the gapless quasi-energy spectrum at Re$E = 0$ under PBC (both PBC and OBC). While $W_\pi = \tilde{W}_\pi = -1$ under all parameters shown in Fig. 3(d), the non-Bloch winding number $\tilde{W}_0$ takes quantized values only in gapped regions under the OBC. Most importantly, the non-Bloch winding number $\tilde{W}_0$ is quantized, and correctly predicts the presence or absence of topological edge states in the gap near Re$E = 0$ [see Figs. 2 and 3(d)], thereby restoring the bulk-boundary correspondence. We find that edge states in both band gaps are chiral, propagating in a counterclockwise fashion along the boundary, similarly to the Hermitian case.

Furthermore, by introducing the non-Bloch Chern number, defined by replacing (k_x, k_y) in Eq. (5) with $[p_x - i\ln_\epsilon[|\beta(p_x, k_y, t)|], k_y]$, the relation between non-Bloch Floquet winding numbers and the non-Bloch Chern numbers of quasienergy bands remains the same as that in the Hermitian case. For instance, in Figs. 2(i) and 2(j), $\tilde{W}_0 = -1$, and $\tilde{W}_\pi = -1$, leading to vanishing non-Bloch Chern numbers for both bands. Nevertheless, anomalous topological edge states emerge in both quasienergy gaps, dictated by the non-Bloch Floquet winding number. We note that, while the non-Bloch Floquet winding numbers $\tilde{W}_\epsilon$ are well-defined as long as the band gap at Re$E = \epsilon$ remains open, the non-Bloch Chern numbers are only well defined in the case that both gaps are open.

Local Chern Marker. While topological invariants are considered as global characters in the system, local topological markers have recently been identified, for both Hermitian[43–46] and non-Hermitian[47] topological systems, which permit us to distinguish different topological phases using quasi-local probes in real space. Based on the Hermitian construction in Ref. [44], we adopt the following local Chern marker, defined on a single unit cell in the bulk, for our two-dimensional quantum-walk dynamics:

$$c(m) = -\frac{4\pi}{A_{\rm c}}{\rm Im}\sum_{s=A,B}\langle \boldsymbol{r}_{m,s}|\hat{P}\hat{x}\hat{Q}\hat{y}\hat{P}|\boldsymbol{r}_{m,s}\rangle, \quad (6)$$

where $A_{\rm c}$ is the area of a unit cell in real space (see Fig. 1), and $|\boldsymbol{r}_{m,s}\rangle$ is the sublattice state s in the mth unit cell; the operator $\hat{P} = \sum_n |\psi_{n,R}\rangle\langle\psi_{n,L}|$ is the projection onto a given quasienergy band, which now is defined in real space. Here, $|\psi_{n,L(R)}\rangle$ is the nth left (right) eigenstate of the relevant band, with $U|\psi_{n,R}\rangle = \lambda_n|\psi_{n,R}\rangle$ and $U^{\dagger}|\psi_{n,L}\rangle = \lambda^{*}_n|\psi_{n,L}\rangle$, and λ_n is the nth eigenvalue of U. In addition, $\hat{Q} = \hat{I} - \hat{P}$, with the identity operators $\hat{I}$, $\hat{x}$ and $\hat{y}$ are the positional operators. Equation (6) extends the previous definition in Ref. [44] to non-Hermitian settings by considering a biorthorgonal construction, and it is distinct from the local marker in Ref. [47], which is also defined for a non-Hermitian topological system with skin effects. We note that for the periodically driven system considered here, the local Chern marker is in-

sufficient to reconstruct the Floquet winding numbers.

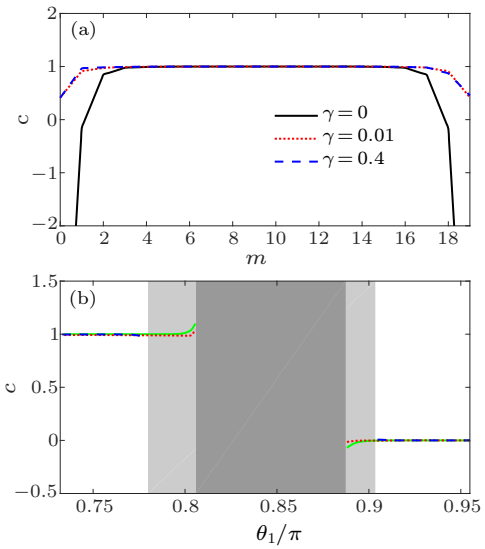

Fig. 4. (a) Spatial dependence of non-Hermitian local Chern markers for different γ. We take $(\theta_1, \theta_2) = (0.78\pi, 1.59\pi)$ for our calculation. We choose the unit cells as shown in Fig. 1, with a system size of $L_x \times L_y = 40 \times 40$, where m is the cell index along the x direction. We adopt the OBC in the x direction and PBC in the y direction. (b) Local Chern marker in the bulk (at the center of a finite system) as a function of θ_1, with $\theta_2 = 1.59\pi$ and $\gamma = 0.4$. The green solid, red dotted, and blue dashed lines represent the non-Hermitian local Chern marker, the non-Bloch Chern number, and the Bloch Chern number, respectively.

Under OBC along the x direction, the local Chern marker should be a function of position in the x direction, as shown in Fig. 4 under fixed parameters, where $\tilde{W}_0 = 0$ and $\tilde{W}_\pi = -1$. The calculated local Chern maker is $\sim$1 sufficiently far from the boundaries, consistent with the non-Bloch Chern number of the corresponding quasienergy band. Deviations are observed close to the boundary, akin to the behavior of a local Chern marker in a Hermitian topological system.[44] We then show the variation of the non-Hermitian local Chern number across the topological phase transition [see Fig. 4]. Here, the Chern marker is quantized to the non-Bloch Chern number calculated via Eq. (5), provided that the quasienergy gap remains open.

Following the practice in Ref. [44], we rewrite Eq. (6) as

$$c(m) = -\frac{4\pi}{A_c}\mathrm{Im}\sum_{s=A,B}\sum_{o,l}\sum_{p,q=A,B} x_{o,p}y_{l,q} \langle \boldsymbol{r}_{m,s}|\hat{P}|\boldsymbol{r}_{o,p}\rangle\langle \boldsymbol{r}_{o,p}|\hat{Q}|\boldsymbol{r}_{l,q}\rangle\langle \boldsymbol{r}_{l,q}|\hat{P}|\boldsymbol{r}_{m,s}\rangle, \quad (7)$$

where the completeness relations $\sum_{o,p}|\boldsymbol{r}_{o,p}\rangle\langle \boldsymbol{r}_{o,p}| = \hat{I}$ are inserted, and $x_{o,p}$ ($y_{l,q}$) corresponds to the x (y) coordinate of the sublattice site p (q) in the oth (lth) unit cell. Based on Eq. (7), it is clear that measuring $c(m)$ amounts to probing, in real space, quantities such as $\langle \boldsymbol{r}_{m,s}|\hat{P}|\boldsymbol{r}_{o,p}\rangle$, which we find decays exponentially over the distance between the mth and oth unit cells, when both band gaps are open and the Chern number of the corresponding quasienergy band is well-defined. Our results therefore suggest the possibility of constructing non-Bloch topological invariants from quasi-local measurements in the bulk. For instance, quantities such as $\langle \boldsymbol{r}_{m,s}|\hat{P}|\boldsymbol{r}_{o,p}\rangle$ may be probed using interference-based measurements.[48] Alternatively, the quantity $\langle \boldsymbol{r}_{m,s}|\hat{P}|\boldsymbol{r}_{o,p}\rangle$ breaks down to a summation of single-particle-density-matrix elements: $\sum_n \langle \boldsymbol{r}_{m,s}|\psi_{n,R}\rangle\langle\psi_{n,L}|\boldsymbol{r}_{o,p}\rangle$, each of which can be constructed by means of full-state tomography. We leave the detailed construction of a detection scheme to future studies.

In summary, we have shown that the non-Bloch band theory is crucial in establishing a non-Hermitian bulk-boundary correspondence for two-dimensional, discrete-time quantum walks. The resulting non-Bloch Floquet winding numbers, defined over the generalized Brillouin zone, correctly predict the emergence of topological edge states in the quasienergy gaps, and are related to the non-Bloch Chern numbers of the corresponding bands. A non-Hermitian local Chern marker is then introduced to characterize non-Bloch Chern numbers in real space, whose quasi-local nature holds the potential for detecting non-Bloch topological invariants in future experiments. Our results should be applicable to general non-Hermitian Floquet topological systems.

We thank Tian-Shu Deng for helpful discussions.

References

[1] Carmichael H J 1993 *Phys. Rev. Lett.* **70** 2273
[2] Lee T E 2016 *Phys. Rev. Lett.* **116** 133903
[3] Kunst F K, Edvardsson E, Budich J C and Bergholtz E J 2018 *Phys. Rev. Lett.* **121** 026808
[4] McDonald A, Pereg-Barnea T and Clerk A A 2018 *Phys. Rev. X* **8** 041031
[5] Borgnia D S, Kruchkov A J and Slager R J 2020 *Phys. Rev. Lett.* **124** 056802
[6] Yao S and Wang Z 2018 *Phys. Rev. Lett.* **121** 086803
[7] Yao S, Song F and Wang Z 2018 *Phys. Rev. Lett.* **121** 136802
[8] Yokomizo K and Murakami S 2019 *Phys. Rev. Lett.* **123** 066404
[9] Yang Z S, Zhang K, Fang C and Hu J P 2020 *Phys. Rev. Lett.* **125** 226402
[10] Zhang K, Yang Z and Fang C 2020 *Phys. Rev. Lett.* **125** 126402
[11] Martinze Alvarez V M, Barrios Vargas J E and Foa Torres L E F 2018 *Phys. Rev. B* **97** 121401(R)
[12] Zhang X Z and Gong J B 2020 *Phys. Rev. B* **101** 045415
[13] Zeng Q B, Yang Y B and Xu Y 2020 *Phys. Rev. B* **101** 020201(R)
[14] Okuma N, Kawabata K, Shiozaki K and Sato M 2020 *Phys. Rev. Lett.* **124** 086801
[15] Wang X R, Guo C X and Kou S P 2020 *Phys. Rev. B* **101** 121116(R)
[16] Lee C H and Thomale R 2019 *Phys. Rev. B* **99** 201103(R)
[17] Song F, Yao S and Wang Z 2019 *Phys. Rev. Lett.* **123**

170401
[18] Helbig T, Hofmann T, Imhof S, Abdelghany M, Klessling T, Molenkamp L W, Lee C H, Szameit A, Greiter M and Thomale R 2020 *Nat. Phys.* **16** 747
[19] Hofmann T, Helbig T, Schindler F, Salgo N, Brzezińska M, Greiter M, Kiessling T, Wolf D, Vollhardt A, Kabaši A, Lee C H, Bilušić A, Thomale R and Neupert T 2020 *Phys. Rev. Res.* **2** 023265
[20] Ghatak A, Brandenbourger M, van Wezel J and Coulais C 2020 *Proc. Natl. Acad. Sci. USA* **117** 29561
[21] Xiao L, Deng T S, Wang K, Zhu G, Wang Z, Yi W and Xue P 2020 *Nat. Phys.* **16** 761
[22] Weidemann S, Kremer M, Helbig T, Hofmann T, Stegmaier A, Greiter M, Thomale R and Szameit A 2020 *Science* **368** 311
[23] Kitagawa T, Rudner M S, Berg E and Demler E 2010 *Phys. Rev. A* **82** 033429
[24] Kitagawa T, Berg E, Rudner M and Demler E 2010 *Phys. Rev. B* **82** 235114
[25] Cayssol J, Dora B, Simon F and Moessner R 2013 *Phys. Status Solidi RRL* **7** 101
[26] Barkhofen S, Nitsche T, Elster F, Lorz L, Gábris A, Jex I and Silberhorn C 2017 *Phys. Rev. A* **96** 033846
[27] Asbóth J K and Obuse H 2013 *Phys. Rev. B* **88** 121406(R)
[28] Broome M A, Fedrizzi A, Lanyon B P, Kassal I, Aspuru-Guzik A and White A G 2010 *Phys. Rev. Lett.* **104** 153602
[29] Kitagawa T, Broome M A, Fedrizzi A, Rudner M S, Berg E, Kassal I, Aspuru-Guzik A, Demler E and White A G 2012 *Nat. Commun.* **3** 882
[30] Zeuner J M, Rechtsman M C, Plotnik Y, Lumer Y, Nolte S, Rudner M S, Segev M and Szameit A 2015 *Phys. Rev. Lett.* **115** 040402
[31] Zhan X, Xiao L, Bian Z, Wang K, Qiu X, Sanders B C, Yi W and Xue P 2017 *Phys. Rev. Lett.* **119** 130501
[32] Xiao L, Zhan X, Bian Z H, Wang K K, Zhang X, Wang X P, Li J, Mochizuki K, Kim D, Kawakami N, Yi W, Obuse H, Sanders B C and Xue P 2017 *Nat. Phys.* **13** 1117
[33] Chen C, Ding X, Qin J, He Y, Luo Y H, Chen M C, Liu C, Wang X L, Zhang W J, Li H, You L X, Wang Z, Wang D W, Sanders B C, Lu C Y and Pan J W 2018 *Phys. Rev. Lett.* **121** 100502
[34] Cardano F, Maffei M, Massa F, Piccirillo B, de Lisio C, De Filippis G, Cataudella V, Santamato E and Marrucci L 2016 *Nat. Commun.* **7** 11439
[35] Cardano F, Errico A D, Dauphin A, Maffei M, Piccirillo B, de Lisio C, De Filippis G, Santamato V C E, Marrucci L, Lewenstein M and Massignan P 2017 *Nat. Commun.* **8** 15516
[36] Rudner M S, Lindner N H, Berg E and Levin M 2013 *Phys. Rev. X* **3** 031005
[37] Zhou L W and Gong J B 2018 *Phys. Rev. B* **98** 205417
[38] Zhou L W and Pan J X 2019 *Phys. Rev. A* **100** 053608
[39] Xie D, Deng T S, Xiao T, Gou W, Chen T, Yi W and Yan B 2020 *Phys. Rev. Lett.* **124** 050502
[40] Schreiber A, Gábris A, Rohde P P, Laiho K, Štefaňák M, Potoček V, Hamilton C, Jex I and Silberhorn C 2012 *Science* **336** 55
[41] Kawabata K, Shiozaki K, Ueda M and Sato M 2019 *Phys. Rev. X* **9** 041015
[42] Yao S, Yan Z and Wang Z 2017 *Phys. Rev. B* **96** 195303
[43] Bianco R and Resta R 2011 *Phys. Rev. B* **84** 241106(R)
[44] Caio M D, Möller G, Cooper N R and Bhaseen M J 2019 *Nat. Phys.* **15** 257
[45] Privitera L and Santoro G E 2016 *Phys. Rev. B* **93** 241406(R)
[46] Pozo O, Repellin C and Grushin A G 2019 *Phys. Rev. Lett.* **123** 247401
[47] Song F, Yao S and Wang Z 2019 *Phys. Rev. Lett.* **123** 246801
[48] Wang K, Qiu X, Xiao L, Zhan X, Bian Z, Sanders B C, Yi W and Xue P 2019 *Nat. Commun.* **10** 2293

Supplemental Material: Two-dimensional quantum walk with non-Hermitian skin effects

Tianyu Li,[1] Yong-Sheng Zhang,[1,2,*] and Wei Yi[1,2,†]

[1] *CAS Key Laboratory of Quantum Information, University of Science and Technology of China, Hefei 230026, China*

[2] *CAS Center For Excellence in Quantum Information and Quantum Physics, Hefei 230026, China*

I. THE EFFECTIVE HAMILTONIAN IN MOMENTUM SPACE

The explicit form of the time-dependent, effective Hamiltonian $H(\mathbf{k},t)$ in Eq. (2) is constructed as the following

$$H(\mathbf{k},t)=\left(\begin{bmatrix}0 & b(t)e^{-ik_x}+d(t)e^{-ik_y}\\ a(t)e^{-ik_x}+c(t)e^{-ik_y} & 0\end{bmatrix}+H.c.\right)+\begin{bmatrix}\gamma(t) & 0\\ 0 & -\gamma(t)\end{bmatrix}, \tag{S1}$$

with the step-wise, time-dependent parameters [1]

$$a(t)=i(\frac{\pi}{2}-\theta_1)G(t-\frac{1}{10}), \tag{S2}$$

$$b(t)=-i\theta_2 G(t-\frac{3}{10}), \tag{S3}$$

$$\gamma(t)=i\gamma G(t-\frac{5}{10}), \tag{S4}$$

$$c(t)=i\theta_2 G(t-\frac{7}{10}), \tag{S5}$$

$$d(t)=i\theta_1 G(t-\frac{9}{10}), \tag{S6}$$

$$G(t)=5\Theta(t+\frac{1}{10})\Theta(\frac{1}{10}-t). \tag{S7}$$

Here $\Theta(t)$ is the Heaviside step function. The time-dependent coefficients divide one Floquet period into five segments, each implementing a gate operation.

II. GENERALIZED BRILLOUIN ZONE

We now outline the recipe for calculating the generalized Brillouin zone, which is encoded in $\beta(p_x,k_y,t)$ under open boundary conditions. Following Eq. (3) in the main text, we have

$$U_\epsilon(\mathbf{k},t)=\begin{cases}e^{-iH_1(\mathbf{k})10t}, & 0\le t\le\frac{1}{10}\\ e^{-iH_2(\mathbf{k})10(t-\frac{1}{10})}e^{-iH_1(\mathbf{k})}, & \frac{1}{10}<t\le\frac{2}{10}\\ e^{-im(\mathbf{k})10(t-\frac{2}{10})}e^{-iH_2(\mathbf{k})}e^{-iH_1(\mathbf{k})}, & \frac{2}{10}<t\le\frac{3}{10}\\ e^{-iH_3(\mathbf{k})10(t-\frac{3}{10})}e^{-im(\mathbf{k})}e^{-iH_2(\mathbf{k})}e^{-iH_1(\mathbf{k})}, & \frac{3}{10}<t\le\frac{4}{10}\\ e^{-iH_4(\mathbf{k})10(t-\frac{4}{10})}e^{-iH_3(\mathbf{k})}e^{-im(\mathbf{k})}e^{-iH_2(\mathbf{k})}e^{-iH_1(\mathbf{k})}, & \frac{4}{10}<t\le\frac{5}{10}\\ e^{-iH_\epsilon^{\rm eff}(\mathbf{k})(2-2t)}, & \frac{1}{2}<t\le 1\end{cases} \tag{S8}$$

where

$$H_1(\mathbf{k}) = (\frac{\pi}{2} - \theta_1) \begin{pmatrix} 0 & -ie^{ik_x} \\ ie^{-ik_x} & 0 \end{pmatrix}, \tag{S9}$$

$$H_2(\mathbf{k}) = -\theta_2 \begin{pmatrix} 0 & ie^{-ik_x} \\ -ie^{ik_x} & 0 \end{pmatrix}, \tag{S10}$$

$$m(\mathbf{k}) = i\gamma \begin{pmatrix} 1 & 0 \\ 0 & -1 \end{pmatrix}, \tag{S11}$$

$$H_3(\mathbf{k}) = \theta_2 \begin{pmatrix} 0 & -ie^{ik_y} \\ ie^{-ik_y} & 0 \end{pmatrix}, \tag{S12}$$

$$H_4(\mathbf{k}) = \theta_1 \begin{pmatrix} 0 & ie^{-ik_y} \\ -ie^{ik_y} & 0 \end{pmatrix}. \tag{S13}$$

The step-wise $H(\mathbf{k}, t)$ and $U_\epsilon(\mathbf{k}, t)$ lead to a time-dependent $\beta(p_x, k_y, t)$ that is also step-wise in its functional form. As an example, we show the calculation β for $t \in (\frac{2}{5}, \frac{1}{2}]$.

With open boundaries in the x direction, k_y is still a good quantum number, and system is reduced to a one-dimensional quantum walk with an additional parameter k_y. Fourier transforming Eq. (S8) over k_x, we find the time-period operator for the reduced one-dimensional quantum walk within the time interval $t \in (\frac{2}{5}, \frac{1}{2}]$

$$U_\epsilon(k_y, t) = \sum_m |m, A\rangle\langle m, A| \otimes \bar{A} + |m, B\rangle\langle m, B| \otimes \bar{B} + \tag{S14}$$

$$|m, A\rangle\langle m, B| \otimes \bar{C} + |m, B\rangle\langle m, A| \otimes \bar{D} + \tag{S15}$$

$$|m, B\rangle\langle m+1, A| \otimes \bar{E} + |m+1, A\rangle\langle m, B| \otimes \bar{F} + \tag{S16}$$

$$|m, A\rangle\langle m+1, A| \otimes \bar{G} + |m+1, A\rangle\langle m, A| \otimes \bar{H} + \tag{S17}$$

$$|m-1, B\rangle\langle m, B| \otimes \bar{J} + |m, B\rangle\langle m-1, B| \otimes \bar{K}, \tag{S18}$$

where $|m, A\rangle$ labels sublattice site A of the m the unit cell along x, and

$$\bar{A} = \sin\theta_1 \cos\theta_2 A_1 A_2 M_1, \tag{S19}$$

$$\bar{B} = \sin\theta_1 \cos\theta_2 B_1 B_2 M_2, \tag{S20}$$

$$\bar{C} = A_1 A_2 M_1 (-\cos\theta_1 \cos\theta_2 P_1 + \sin\theta_1 \sin\theta_2 P_0), \tag{S21}$$

$$\bar{D} = B_1 B_2 M_2 (\cos\theta_1 \cos\theta_2 P_1 - \sin\theta_1 \sin\theta_2 P_0), \tag{S22}$$

$$\bar{E} = B_1 B_2 M_2 (-\cos\theta_1 \cos\theta_2 P_0 + \sin\theta_1 \sin\theta_2 P_1), \tag{S23}$$

$$\bar{F} = A_1 A_2 M_1 (\cos\theta_1 \cos\theta_2 P_0 - \sin\theta_1 \sin\theta_2 P_1), \tag{S24}$$

$$\bar{G} = A_1 A_2 M_1 (-\cos\theta_1 \sin\theta_2 P_0), \tag{S25}$$

$$\bar{H} = A_1 A_2 M_1 (-\cos\theta_1 \sin\theta_2 P_1), \tag{S26}$$

$$\bar{J} = B_1 B_2 M_2 (-\cos\theta_1 \sin\theta_2 P_1), \tag{S27}$$

$$\bar{K} = B_1 B_2 M_2 (-\cos\theta_1 \sin\theta_2 P_0) \tag{S28}$$

with

$$M_1=\begin{pmatrix}e^{\gamma} & 0\\ 0 & e^{-\gamma}\end{pmatrix}, M_2=\begin{pmatrix}e^{-\gamma} & 0\\ 0 & e^{\gamma}\end{pmatrix}, P_0=\begin{pmatrix}1 & 0\\ 0 & 0\end{pmatrix}, P_1=\begin{pmatrix}0 & 0\\ 0 & 1\end{pmatrix},$$
$$A_1=\begin{pmatrix}\cos\theta_1^{'} & \sin\theta_1^{'}e^{-ik_y}\\ -\sin\theta_1^{'}e^{ik_y} & \cos\theta_1^{'}\end{pmatrix}, B_1=\begin{pmatrix}\cos\theta_1^{'} & -\sin\theta_1^{'}e^{ik_y}\\ \sin\theta_1^{'}e^{-ik_y} & \cos\theta_1^{'}\end{pmatrix},$$
$$A_2=\begin{pmatrix}\cos\theta_2 & -\sin\theta_2 e^{ik_y}\\ \sin\theta_2 e^{-ik_y} & \cos\theta_2\end{pmatrix}, B_2=\begin{pmatrix}\cos\theta_2 & \sin\theta_2 e^{-ik_y}\\ -\sin\theta_2 e^{ik_y} & \cos\theta_2\end{pmatrix}. \tag{S29}$$

Here $\theta_1^{'}=(10t-4)\theta_1$, for $t\in(\frac{2}{5},\frac{1}{2}]$.

Assuming a bulk state ansatz

$$|\psi\rangle=\sum_m \beta^{-2m}(|m,A\rangle\otimes|\phi\rangle+\beta^{-1}|m,B\rangle\otimes\sigma_x|\phi\rangle), \tag{S30}$$

we have

$$U_\epsilon(k_y,t)|\psi\rangle=\sum_m \beta^{-2m}(|m,A\rangle\otimes(\bar{A}+\beta^{-1}\bar{C}\sigma_x)+|m,B\rangle\otimes(\bar{D}+\beta^{-1}\bar{B}\sigma_x)+|m+1,A\rangle\otimes(\bar{H}+\beta^{-1}\bar{F}\sigma_x) \tag{S31}$$
$$+|m+1,B\rangle\otimes(\beta^{-1}\bar{K}\sigma_x)+|m-1,B\rangle\otimes(\bar{E}+\beta^{-1}\bar{J}\sigma_x)+|m-1,A\rangle\otimes\bar{G})|\phi\rangle \tag{S32}$$
$$=\lambda\sum_m \beta^{-2m}(|m,A\rangle\otimes|\phi\rangle+\beta^{-1}|m,B\rangle\otimes\sigma_x|\phi\rangle). \tag{S33}$$

Non-trivial solution of the eigen equation above exists only if

$$\det(\bar{A}-\lambda+\beta^{-1}\bar{C}\sigma_x+\beta^{-2}\bar{G}+\beta\bar{F}\sigma_x+\beta^2\bar{H})=0. \tag{S34}$$

At any given instant within the time range $(\frac{2}{5},\frac{1}{2}]$, we numerically solve the eigen spectum λ of an open chain, from which we get four non-zero solutions β using Eq. (S34). We sort these solutions as $|\beta_1|\le|\beta_2|\le|\beta_3|\le|\beta_4|$. The condition of $|\beta_2|=|\beta_3|$ fixes the generalized Brillouin zone [2].

The calculation of β in other time intervals are similar. In particular, for $t\in(\frac{1}{2},1]$, β is independent of time.

* yshzhang@ustc.edu.cn
† wyiz@ustc.edu.cn

[1] J K Asboth and J M Edge 2015 Phys. Rev. A **91** 022324
[2] K Yokomizo and S Murakami 2019 Phys. Rev. Lett. **123** 066404